



**HAL**  
open science

# Calibration of the Interaction Soil Biosphere Atmosphere land-surface scheme on a small tropical high-mountain basin (Cordillera Real, Bolivia)

Yvan Caballero, Pierre Chevallier, Aaron Boone, Joël Noilhan, Florence  
Habets

► **To cite this version:**

Yvan Caballero, Pierre Chevallier, Aaron Boone, Joël Noilhan, Florence Habets. Calibration of the Interaction Soil Biosphere Atmosphere land-surface scheme on a small tropical high-mountain basin (Cordillera Real, Bolivia). *Water Resources Research*, 2007, 43 (7), 10.1029/2005WR004490 . hal-01922072

**HAL Id: hal-01922072**

**<https://hal.science/hal-01922072>**

Submitted on 26 Mar 2021

**HAL** is a multi-disciplinary open access archive for the deposit and dissemination of scientific research documents, whether they are published or not. The documents may come from teaching and research institutions in France or abroad, or from public or private research centers.

L'archive ouverte pluridisciplinaire **HAL**, est destinée au dépôt et à la diffusion de documents scientifiques de niveau recherche, publiés ou non, émanant des établissements d'enseignement et de recherche français ou étrangers, des laboratoires publics ou privés.

## Calibration of the Interaction Soil Biosphere Atmosphere land-surface scheme on a small tropical high-mountain basin (Cordillera Real, Bolivia)

Yvan Caballero,<sup>1</sup> Pierre Chevallier,<sup>2</sup> Aaron Boone,<sup>3</sup> Joël Noilhan,<sup>3</sup> and Florence Habets<sup>4</sup>

Received 6 August 2005; revised 1 March 2007; accepted 6 April 2007; published 17 July 2007.

[1] In a continuing effort to test the behavior of Meteo France's land-surface scheme, Interaction Soil Biosphere Atmosphere (ISBA), under a wide range of hydrometeorological conditions, the scheme was applied to a small tropical high-mountain river basin of the Cordillera Real in Bolivia. The surface scheme simulates the key hydrological processes, such as evaporation, infiltration, surface runoff, and snow and soil ice freeze-thaw processes, which are essential for accurately simulating the hydrological behavior of the river basin in this type of location. The 12.5 km<sup>2</sup> nonglacierized subbasin has been divided into homogeneous surface units with irregular shapes, on the basis of their elevation and soil surface characteristics. The ISBA scheme was applied to each unit and the water fluxes were transferred from one unit to another using a system dynamics modeling approach. The method was applied step by step, improving its efficiency based on several hypotheses. This special application of the ISBA scheme, combining the high-mountain conditions and the tropical seasonality is discussed.

**Citation:** Caballero, Y., P. Chevallier, A. Boone, J. Noilhan, and F. Habets (2007), Calibration of the Interaction Soil Biosphere Atmosphere land-surface scheme on a small tropical high-mountain basin (Cordillera Real, Bolivia), *Water Resour. Res.*, 43, W07423, doi:10.1029/2005WR004490.

### 1. Introduction

[2] The impact of climate change on the water resources in mountainous regions, where the cryospheric cover plays a significant role, is a major concern for the scientific community in climate and water sciences [Barnett *et al.*, 2005]. The main challenge is to transfer the results of the global approach given by General Circulation Models to the local scale to satisfy the following interests of water resource users: domestic water supply, industry, energy supply, and agriculture. In France, several studies have been conducted in the Alps and the Pyrenees [Habets *et al.*, 1999a; Etchevers *et al.*, 2001; Voirin-Morel, 2003] on the basis of the French Meteorological Research Centre's modeling system using, for the basin scale, the Interaction Soil Biosphere Atmosphere (ISBA) land-surface scheme on a regular grid.

[3] The ISBA land-surface scheme [Noilhan and Planton, 1989; Noilhan and Mahfouf, 1996], a component of the French forecast model, ARPEGE-Climat [Royer *et al.*, 2002], has been tested and refined over the last 15 years. It has been evaluated within international comparison programs in off-line mode, i.e., decoupled from the parent atmospheric model and driven using prescribed atmospheric forcing. These pro-

grams include the "Project for Intercomparison of Landsurface Parameterization Schemes" [Henderson-Sellers *et al.*, 1993; Henderson-Sellers *et al.*, 1995; Wood *et al.*, 1998; Schlosser *et al.*, 2000; Bowling *et al.*, 2003], the "Global Soil Wetness Project," [Dirmeyer *et al.*, 1999], and the "Rhône-AGGregation Experiment" [Boone *et al.*, 2004].

[4] The ISBA land-surface scheme was tested on a wide range of spatial scales. Local-scale studies were conducted to study particular hydrological processes [Mahfouf and Noilhan, 1996; Calvet *et al.*, 1998; Boone *et al.*, 1999], and basin-scale studies provided modeling tools for river discharge simulation [Habets *et al.*, 1999b, 1999c]. The addition of a representation of snow [Douville *et al.*, 1995; Boone and Etchevers, 2001] and soil freezing [Boone *et al.*, 2000] made it possible to apply the scheme to mountainous basins and provide water management or climate change impact assessments [Habets *et al.*, 1999a; Etchevers *et al.*, 2001; Voirin-Morel, 2003; Caballero *et al.*, 2007].

[5] In a continuation of the studies done in the Alps, Caballero *et al.* [2004] applied the ISBA scheme in the mountainous context of the Andes chain in Bolivia. In this study, ISBA was integrated into a system dynamics model in order to simulate the river discharge at the outlet of a basin containing a hydropower system located on the upper part of an Amazonian tributary called the Zongo River (Figure 1).

[6] In the previous applications, ISBA was used on large regular cells (generally 8 × 8 km) with a good-quality distributed climatic data set. In the very high altitudes of the Andes, several studies [Ribstein *et al.*, 1995; Wagnon *et al.*, 1999; Francou *et al.*, 2000; Favier *et al.*, 2004; Sicart *et al.*, 2005] have shown the fundamental role of the energy

<sup>1</sup>Bureau de Recherche Géologique et Minière Corse, Bastia, France.

<sup>2</sup>Institut de Recherche pour le Développement Great Ice, Montpellier, France.

<sup>3</sup>Centre National de Recherches Météorologiques Météo-France, Toulouse, France.

<sup>4</sup>UMR Sysiphe, CNRS, Université Pierre et Marie Curie, Paris, France.

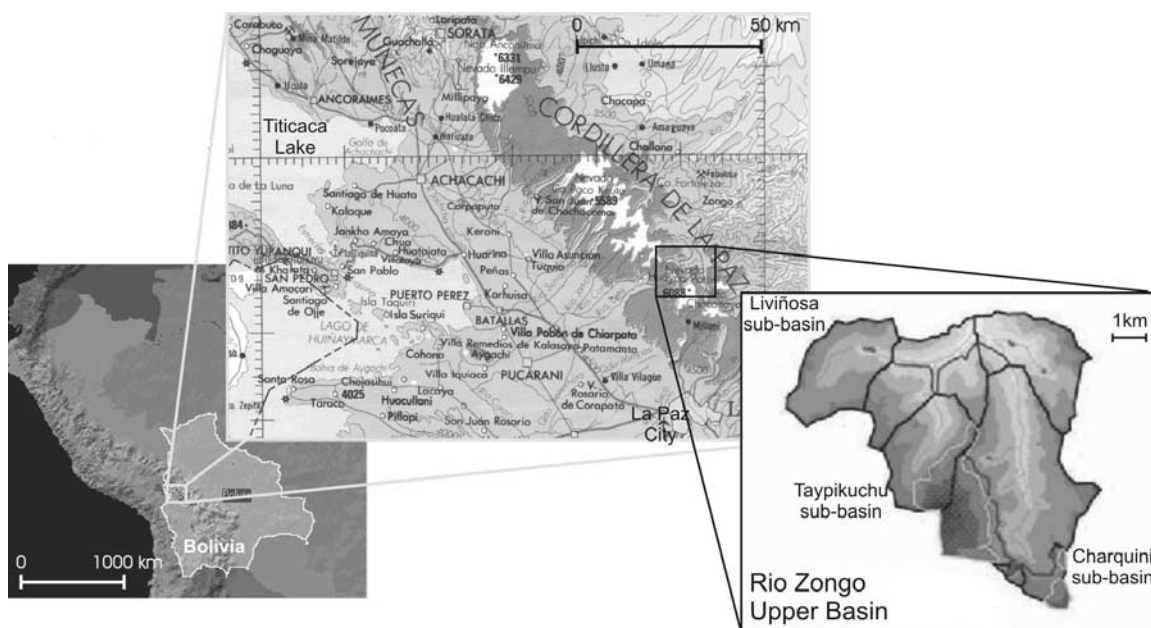


**Figure 1.** Location map of the study site in Bolivia.

balance interactions, related to the surface patterns and the specific meteorological forcing, taking into account the variability of the snow cover. Applying ISBA to this context was found to provide a good opportunity to test the scheme in tropical high-mountain hydrometeorological conditions and at small scales adapted to the basin's morphology (slopes and land/snow and ice cover).

[7] The present paper aims to complete the 2004 paper, by detailing and discussing the application of the ISBA scheme, combined with a simple routing procedure, to a small watershed characterized by a land cover pattern of irregular small units, steep slopes, the strong influence of the radiative fluxes due to the very high elevation, and a pronounced seasonality including snow and rain precipitations.

[8] After a general description of the main features of the ISBA scheme, with an emphasis on runoff, soil water content evolution, drainage and snow parameterizations, and a presentation of the local meteorological conditions, the calibration and validation of the scheme on the Liviñosa watershed is detailed. Since the paper focuses on methodology, the authors chose to describe it step by step, presenting the results obtained with the problems encountered, without necessarily attempting to resolve all these issues but rather explain the hypotheses used to advance the model.

## 2. Methods and Context

### 2.1. ISBA Land-Surface Scheme

#### 2.1.1. General Description

[9] ISBA simulates the water and energy exchanges between the composite soil-vegetation surface and the atmospheric boundary layer, the changes in soil water content and snowpack, and the runoff and deep drainage fluxes. Different options can be used depending on the study's objectives. The simplest configuration is based on the force-restore temperature and soil water content evolution method [Deardorff, 1977, 1978]. Deardorff simulated

soil moisture evolution by applying the precipitation and evaporation forcing to the soil surface and restoring the soil moisture deep layer profile by vertical diffusion. The ISBA-Force Restore version [Noilhan and Planton, 1989; Noilhan and Mahfouf, 1996] thus resolves an energy budget for the soil-vegetation complex by relating the thermal and hydrological properties to the soil texture and the vegetation type, which are the primary parameters of the model. The secondary parameters are calculated using continuous relations as a function of the primary parameters [Noilhan and Lacarrère, 1995].

[10] A later version called ISBA-3L (for three soil layers) [Boone et al., 1999], which was used for this study, distinguishes a root zone layer, which improves the simulation of evaporation and runoff (Figure 2). This version was used together with the explicit snow scheme option [Boone and Etchevers, 2001]. Therefore the time evolution of the following variables was calculated; a surface and a deep-soil temperature, four snow cover variables (albedo, enthalpy, density, and snow water liquid equivalent; the latter three were computed for three layers), the soil liquid water content (three layers), and the soil liquid water equivalent ice content (two layers).

#### 2.1.1.1. Subgrid Runoff

[11] In theory, runoff can be obtained either by saturation of the soil's water storage capacity [Dunne and Black, 1970] or when the rainfall intensity is greater than the infiltration capacity of the soil surface [Horton, 1945]. However, this parameterization cannot be easily used at a regional scale because of the subgrid heterogeneity of, for example, the topography, land use, or rainfall pattern. At this scale, runoff often appears over a grid fraction before the whole surface reaches the conditions needed to generate overland flow using the above mentioned parameterizations. This is why a subgrid runoff parameterization was introduced into ISBA [Habets et al., 1999b]. It is based on a statistical distribution of the spatial variability of the subgrid infiltration capacity

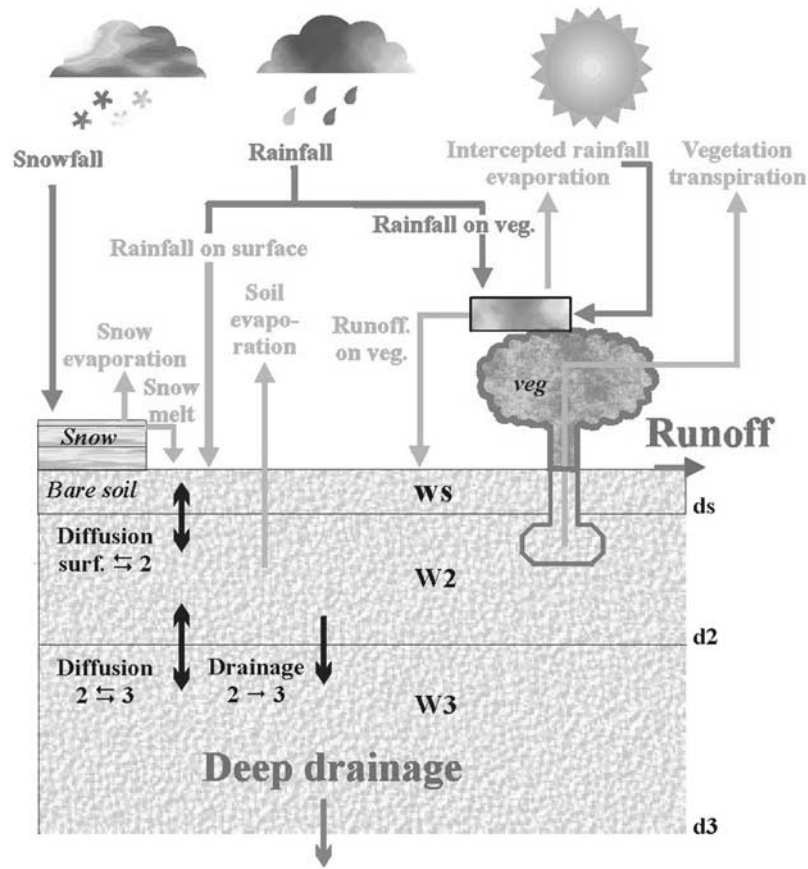


**Figure 2.** Schematic description of the hydrological processes simulated by the ISBA land-surface scheme (based on the work of Boone [2000]).  $w_s$ ,  $w_2$ , and  $w_3$  are the soil water content of the  $d_s$ ,  $d_2$ , and  $d_3$  depth layers.

[Dümenil and Todini, 1992; Wood et al., 1992; Flamiglietti and Wood, 1994], depending on the  $w_2$  soil water content, on three soil parameters ( $w_{\text{sat}}$ ,  $w_{\text{wilt}}$ , and  $d_2$ , the saturated and wilting point water content and the root zone thickness, respectively), and a shape parameter called “ $b$ ” that can be a function of topography, soil, and vegetation type. For fixed soil parameters, the subgrid runoff will increase with an increase in  $b$  [Habets et al., 1999b].

#### 2.1.1.2. Subgrid Drainage

[12] When the root or deep layer’s water content is less than the field capacity, a drainage production method, called subgrid drainage, is activated [Habets et al., 1999c]. This mechanism was introduced into ISBA to simulate dry season flows supplied by the temporary water tables and natural reservoirs. It can produce a relatively small linear drainage for soil water content values below the field capacity. The subgrid drainage depends on the soil texture and is on the order of a few millimeters per day. It must be calibrated using observed data from the study zone.

#### 2.1.1.3. Cold Season Processes

[13] The ISBA-Explicit Snow parameterization was used to describe the snow cover dynamics, as this has proven to be critical for mountain hydrology [Boone, 2000; Etchevers, 2000]. A specific energy budget for the snow cover is computed. The snowpack is divided into three layers of varying thickness where the snow water equivalent, density, and stocked heat or enthalpy are simulated. This facilitates the simulation of internal snow cover processes such as

liquid water retention, refreezing of meltwater and rainwater, and a physically based compaction [Boone, 2000; Boone and Etchevers, 2001].

[14] The influence of freezing on the soil water content and the soil surface temperature evolution is also taken into account using the two-layer soil ice option [Boone et al., 2000], which is based on the simpler operational method described by Giard and Bazile [2000], since it improves the simulation of significant freezing for prolonged periods.

## 2.2. Meteorological Context of a Tropical High-Mountain Basin Located in the Bolivian Andes

[15] The study zone, the Liviñosa basin, is a high-mountain nonglacial basin covering an area of 12.5 km<sup>2</sup> (Figure 1), which ranges in altitude from 4150 to 5150 m. It corresponds to the upper part of the Rio Zongo Valley (16°S, 68°W), which is located on the Eastern part of the Andean chain, approximately 30 km north from La Paz, Bolivia. The summits surrounding the valley reach altitudes between 5000 and 6088 m (Huayna Potosi), and some of them are capped by small glaciers which provide meltwater to the Rio Zongo River. Because of their relatively low altitude, there are no glaciers on the Liviñosa basin’s peaks (approximately 5000 m asl). Consequently, the runoff in the basin comes only from snowmelt and rainfall.

[16] The climate in the region is mainly controlled by the position of the Intertropical Convergence Zone, whose oscillations result in a highly pronounced annual variability

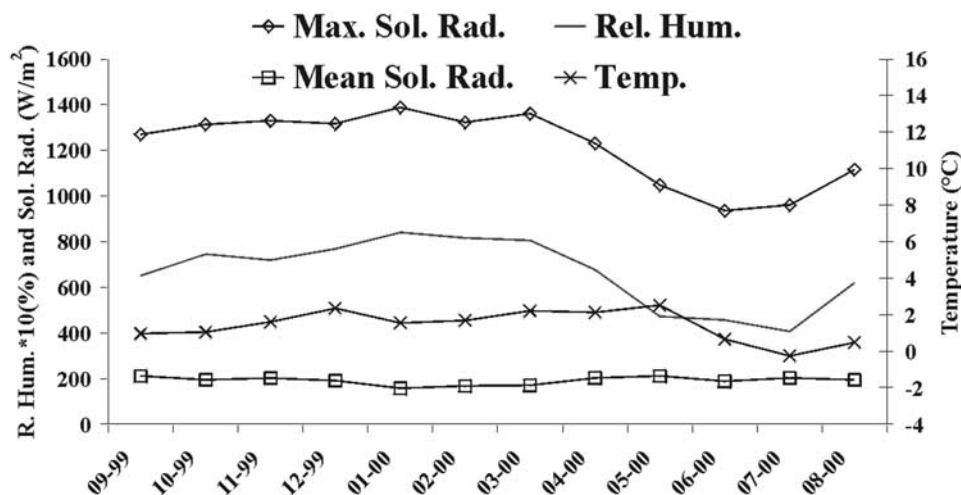


Figure 3. Monthly values of the average and maximum incoming solar radiation, average relative humidity and temperature observed at the Plataforma meteorological station (4750 m).

in the rainy season [Aceituno, 1988; Vuille et al., 2000], which is characterized by a dry and cold season (southern winter, May to September) and a hot and wet season (southern summer, November to March) (Figure 3). The high altitude, the low latitude, and the steep slopes (leading to significant interception of reflected incoming solar radiation at some locations and times) of the area result in an incoming solar radiation that can reach the observed values at the top of the terrestrial atmosphere; rather intense radiative forcing is observed during the entire year. The variations of the climatic daily mean data (solar radiation, temperature, and atmospheric humidity) have been reported for each dry and humid season (Figure 3). As is typical of a tropical climate, it can be noted that the temperature does not vary much between the cold and dry and hot and wet seasons. This figure also shows the strong seasonality of the

atmospheric humidity (around 50% during dry season and 80% for the wet season), which is caused by the nearby sedimentary high and dry Altiplano plateau (mean altitude, 4000 m). This plateau stimulates an atmospheric drying during the southern winter. During the southern summer, the western intertropical winds contribute to a humidity increase by pushing the Amazonian humid air masses against the Andean chain.

[17] The average monthly rainfall, calculated over 29 years at different daily rain gauges of the Zongo river basin, is shown in Figure 4. The precipitation is concentrated in the Southern Hemisphere summer (November to March), and it decreases with altitude. This behavior was found to be similar in all of the subbasins of the upper part of the Zongo river basin [Caballero et al., 2002], and this is the case for the Liviñosa basin. An average monthly altitudinal precipitation

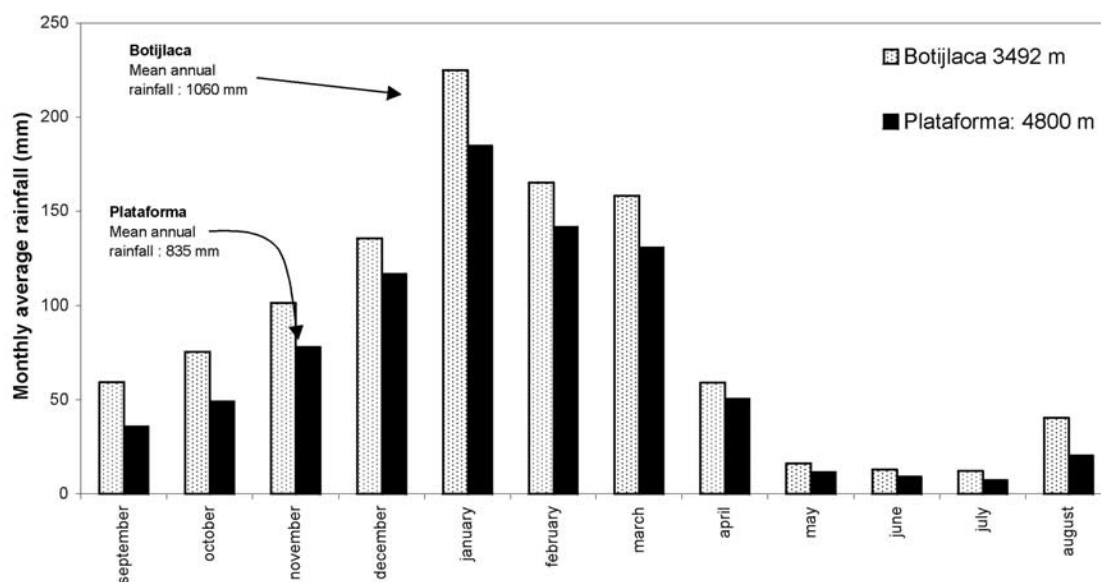


Figure 4. Zongo valley, monthly and annual average cumulated rainfall during a 27-year period (1971–1997) observed at two rain gauges of the Zongo valley, showing the strong seasonality of precipitation, as well as the influence of altitude [Caballero et al., 2002].

**Table 1.** Average Monthly Rainfall Gradient According to the Altitude in the Upper Part of the Zongo Valley, Calculated on the Basis of the 10 Daily Rain Gauge Records Available in the Zongo Valley (Average Value)

	Sept.	Oct.	Nov.	Dec.	Jan.	Feb.	Mar.	Apr.	May	Jun.	Jul.	Aug.
Above 3500 (mm/100 m)	-1.7	-2.1	-1.8	-1.7	-3.6	-2.7	-2.8	-0.4	-0.3	-0.3	-0.3	-1.4
Mean value over the Zongo valley (mm/100 m)	-0.4	-2.8	-3.4	-5.9	-5.2	-6.6	-5.9	-2.4	-1.2	-1.6	-1.9	-1.2

gradient was calculated for the entire Zongo River valley from 10 daily rain gauge records (Table 1). For the upper part of the valley (corresponding to the Liviñosa basin altitude), this gradient appears to be smaller than in the lower part, although it is still negative. It varies from  $-6.6$  mm / 100 m during the summer to  $-0.5$  mm / 100 m during the winter.

[18] The Liviñosa basin geomorphology is typical of the Andean landscapes. Three types of surfaces can be identified (Figure 5): (1) rock faces with both steep and gentles slopes (75% of the total surface area), which are mainly composed of massive metamorphic rocks with no deep infiltration and can be locally covered by a thin layer of soil; (2) slope deposits (23% of the total surface), which are mainly lateral moraine or talus slopes with an average slope of  $40^\circ$  [Caballero *et al.*, 2002], which receive all of the runoff coming from the rock faces; and (3) valley bottom formations (2% of the total surface), which are composed of humid basal moraine and fluvio-glacial deposits overlaid by peat, where the throughflow processes strongly control the discharge generated by the entire basin, despite their relatively small surface area coverage.

### 3. Calibration Methods

#### 3.1. Basin Model

[19] The ISBA land-surface scheme simulates the vertical energy and hydrological fluxes. It is usually applied over a square cell of variable size within which the energy and water budgets are calculated; however, the simulation results for such models depend on the grid scale chosen. For a given surface, a higher grid resolution increases the number of cells needed and increases the calculation time.

This problem can be offset to some extent using a relatively coarse grid together with aggregated soil and vegetation parameters [Noilhan and Lacarrère, 1995]; however, this method can be problematic for the case of large subgrid spatial heterogeneity in terms of both parameters and meteorology [Boone *et al.*, 2004].

[20] The small area of the Liviñosa basin allowed us to build cells corresponding to only one surface type, taking advantage of the spatial distribution in irregular shapes. Eight surface units were used to define the surface of the basin and the runoff network model. They were built by combining the three different types of soil surface described in the previous section (rock faces, slope deposits, and valley bottoms) with 300-m elevation bands (Table 2 and Figure 5). This elevation range was selected because it provides an acceptable compromise between the soil surface description scale (three types of soil surface for a basin with a 1200-m difference in altitude between the peak and the outlet) and the available meteorological measurement precision. Building the surface units in this manner allows us to consider a homogeneous soil surface type within a unit, thereby reducing the subgrid heterogeneity of the soil surface properties. Moreover, a specific atmospheric forcing was calculated for each grid cell of the basin on the basis of the computed altitude gradients.

#### 3.2. Atmospheric Forcing

[21] The atmospheric forcing applied on each unit was calculated as follows:

[22] • Rainfall measured in the only rain gauge available in the area and located at the outlet of the basin was extrapolated to each surface unit using the monthly altitu-

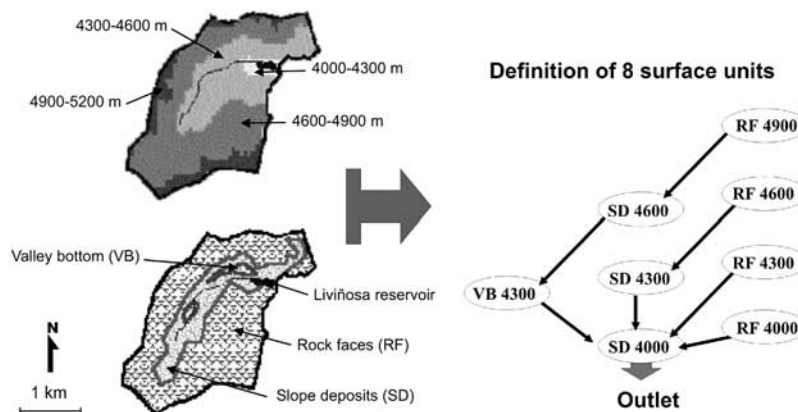


**Figure 5.** Physical and geomorphological characteristics of the Liviñosa river basin landscape, 300-m elevation bands and three types of surface: rock faces, slope deposits, and valley bottom. The Liviñosa reservoir drains the entire runoff of the river basin. Eight surface units were built by crossing the three different types of soil surface with the 300-m elevation bands to describe the runoff network model for the water routing through the river basin. The water flow leaves the basin by the slope deposits 4000 surface unit.

**Table 2.** Distribution of the Eight Selected Surface Units (Bold Numbers) Defined on the Liviñosa Basin With Their Respective Area (in Parenthesis) and the Cumulated Area in Square Kilometers and in Percent of the Basin Area

	Valley Bottom	Slope Deposits	Rock Faces	Surface, km <sup>2</sup>
<b>4000–4300</b>		(0.3)	(0.1)	0.4
<b>4300–4600</b>	(0.3)	(1.9)	(1.5)	3.7
<b>4600–4900</b>		(0.6)	(5.7)	6.4
<b>4900–5200</b>			(2.0)	2.0
Surface, km <sup>2</sup>	0.3	2.9	9.3	<b>12.5</b>
Surface, %	<b>2</b>	<b>23</b>	<b>75</b>	<b>100</b>

dinal gradient given in Table 1. Gaps were completed using rainfall data from neighboring basins, when the data series were sufficiently correlated.

[23] • Snowfall/rainfall distribution was made using a critical atmospheric temperature value. *L'Hôte et al.* [2004] reported a study by *Leblanc* [2001], which found that 50% of the precipitation fell as snow at the Plataforma weather station (4750 m, on the southern boundary of the Zongo basin), for a temperature measured within the range  $[-2^{\circ}\text{C}; -1^{\circ}\text{C}]$ , between 1998 and 2000. In the present study, the critical temperature value was initially set to  $-1.5^{\circ}\text{C}$ . A study of sensitivity of the simulated runoff to the variation in the critical temperature showed later that the runoff simulation quality sharply decreased when the critical

temperature value exceeded  $-1^{\circ}\text{C}$  (see the last paragraph of section 3.5.3).

[24] • The standard atmospheric lapse rate of  $-6.5^{\circ}\text{C}/\text{km}$  [*Barry*, 1992] was used to model the decrease in temperature with altitude. The resulting temperatures were then used to calculate the specific humidity, downwelling atmospheric radiation, and snowfall/rainfall distribution variation with altitude. Specific humidity was calculated as a function of relative humidity and temperature [*Brutsaert*, 1982]. Incident atmospheric radiation was calculated using the formula of *Staley and Jurica* [1972]. Solar radiation and wind speed measured at the Plataforma weather station were considered constant with altitude.

[25] An example of the resulting atmospheric forcing at a 30-min time step is shown in Figure 6.

### 3.3. Parameters of the ISBA Land-Surface Scheme

[26] Tables 3 and 4 show all the main parameters used in the ISBA whose values were determined from field data measured within the study region, a literature review, or calibration (highlighted parameters). Table 4 lists the types of surface-dependent parameters, including the vegetation cover fraction (mainly alpine grassland with foam-covered boulders and low shrubs) that was calculated using the Leaf Area Index (LAI) using relationships from the work of *Habets et al.* [1999b]. It is worth mentioning that at the basin's altitude, the seasonal vegetation-covered area variation can be ignored. At the beginning of the simulation,

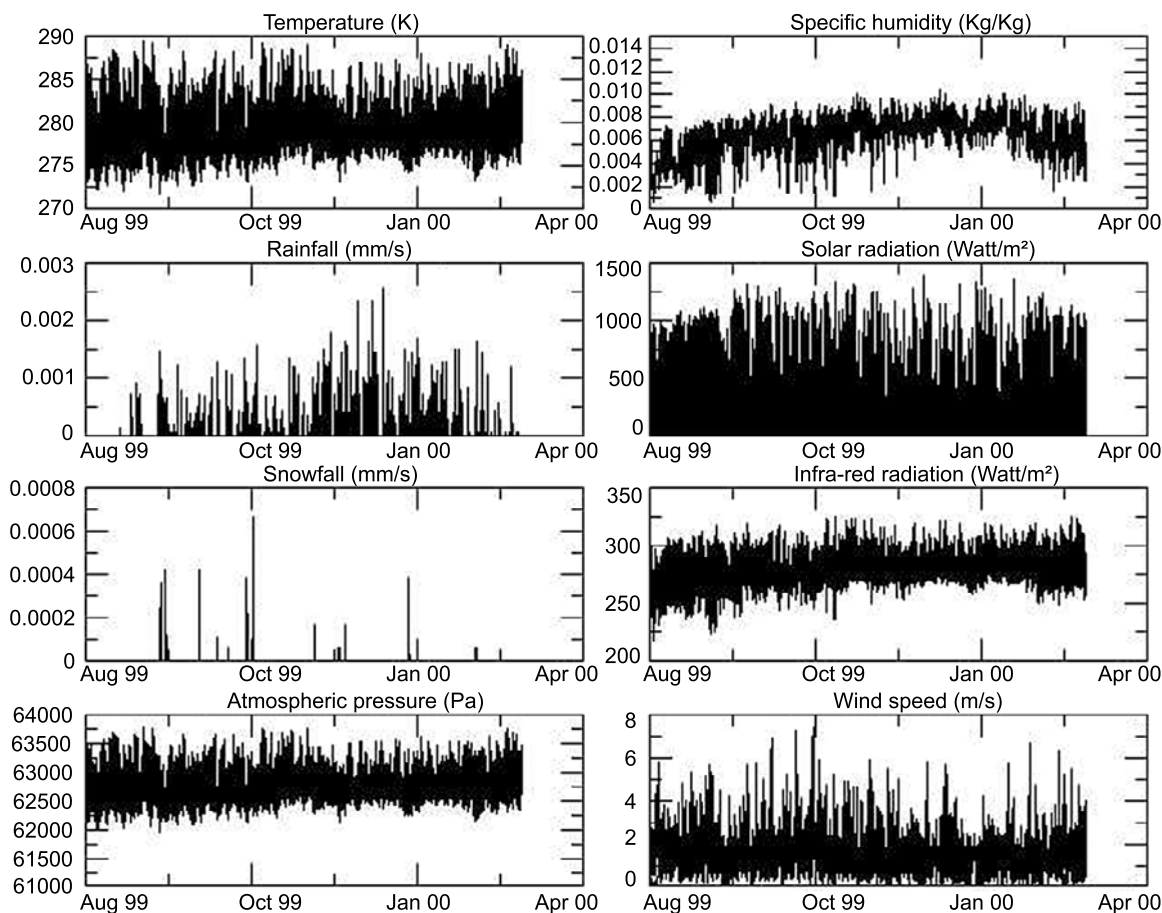


**Figure 6.** Liviñosa basin, atmospheric forcing values over the lowest surface unit (4000–4300 m) at the half-hour time step between 1 August 1999 and 30 April 2000.

**Table 3.** General Parameters for the ISBA's Soil-Vegetation-Snow Cover Description

Vegetation Parameters	Value	Reference
Minimum Stomatic Resistance, $\text{sm}^{-1}$	40	<i>Calvet et al.</i> , 1998; <i>Habets et al.</i> , 1999b
Vegetation's Heat Capacity, $\text{J K}^{-1} \text{m}^{-2}$	2 E-05	Theoretical value
Snow and Ice Parameters	Value	Reference
Initial Volumetric Soil Ice Content, $\text{m}^3 \text{m}^{-3}$	0	Field assumption
Soil Ice Reservoir Depth, m	0.01	<i>Boone et al.</i> , 2000
Initial Snow Cover Water Content Equivalent, mm	0	Field assumption
Initial Snow Cover Density, $\text{kg/m}^3$	100	Fresh snow theoretical value
Initial Snow Albedo (No Dimension)	0.85	Fresh snow theoretical value
Snowmelt Temperature, K	273.15	Theoretical value

root and deep soil depths were fixed a priori verifying that they were consistent with field knowledge. A calibrating adaptation was operated afterward (section 3.5.2). For the rock-face case, only one bulk soil layer was used, meaning that the root zone and the deep soil depths were set to an equal value. The subgrid runoff and drainage parameters were also calibrated for the three surface units represented in the eight cells.

### 3.4. Monitoring Devices and Data Availability

[27] A water level gauge was installed at the outlet of the Liviñosa basin, immediately below the Liviñosa reservoir used to collect water for hydropower production (Figure 5). This device monitored the discharge between August 1999 and April 2001. The river discharges measured between August 1999 and April 2000 were corrected from the influence of reservoir storage or emptying. The reservoir dimensions were calculated in previous studies [*Reinhardt*, 1997], and the water level in the reservoir was measured twice a day. Therefore it was possible to correct the reservoir influence on the runoff data with a simple water volume budget in order to obtain the “natural” runoff data series for the ISBA calibration. This was done for each time step, by considering that the natural discharge was equal to the variation of the water volume stocked in the reservoir, plus the evaporated stocked water, plus the water released from the reservoir, minus the rainfall over the reservoir [*Caballero*, 2001]. The rest of the data (April 2000 to April 2001, with a large gap ranging from January to March 2001) was used for validation.

[28] As stated above in section 3.2, the precipitation was measured at a rain gauge equipped with tipping buckets and located at the outlet of the basin. This rain gauge was not protected against the influence of wind on the precipitation measurement. Several studies have examined the influence of the wind on rainfall measurements [e.g. *Chevallier and Lapetite*, 1986; *Yang et al.*, 1999; *Yang et al.*, 2000; *Chang and Flanery*, 2001]. These studies showed that an average wind speed of 2 m/s underestimates the measured rainfall and snowfall by 10 and 20%, respectively. In the Zongo valley, which is a transition zone between the Amazonian basin and the Andean mountains, a nearly constant wind is often greater than 4 m/s (Figure 6) during the entire year. In the Liviñosa basin, even if the 1999–2000 annual precipitation considered over the whole basin could be considered to be equal to its maximum value (1252 mm, i.e., without considering the decrease in precipitation with altitude; see Table 1), it would still not be enough to produce the measured water flow (1131 mm) at the outlet of the basin during the same period. Indeed, using this hypothesis, only  $1252 - 1131 = 121$  mm would be available for both water storage and evaporation. This value seems to be too far below the regional potential evapotranspiration (estimated at approximately 400 mm by the PHICAB program) [*Roche*, 1982] to be realistic, particularly if it is considered that some of this water would also go into soil water storage. As no reference device was available to estimate the influence of wind speed on the measured rainfall, the parameters were calibrated without correcting the rain gauge data. Once they were calibrated, the model sensitivity

**Table 4.** Surface Dependent Parameter Type<sup>a</sup>

Parameter/Surface Type	Valley Bottom	Slope Deposit	Rock Face
Soil Texture (% of clay)	0.3	0.15	0.03
Soil Texture (% of sand)	0.4	0.2	0.96
Root Zone Depth (D2, m)	0.5	0.5	*1.0
Deep Zone Depth (D3, m)	1.0	1.0	*1.0
Subgrid Runoff Coefficient ( <i>b</i> )	*0.01	*0.01	*0.01
Subgrid Drainage Coefficient (wdrain)	*0.0	*0.0	*0.0
Three-Layer Initial Soil Water Content, $\text{m}^3/\text{m}^3$	Wilting point	Wilting point	Wilting point
Albedo (H99)	0.2	0.2	0.2
Leaf Area Index (LAI, $\text{m}^2 \text{m}^{-2}$ ) (H99)	1.5	0.5	0.0
Vegetation cover grid fraction ( $f^2$ LAI)	0.59	0.26	0.0
Vegetation Rugosity, m (H99)	0.1	0.1	0.01

<sup>a</sup>(H99) means that the parameter's values were based on the study by *Habets et al.* [1999a]. Those in shaded cells and preceded by an asterisk are the default value and were calibrated. The vegetation cover grid fraction was computed using the equation  $\text{VEG} = 1 - \exp(-\alpha \text{ LAI})$  taken from the work of *Habets et al.* [1999c], where  $\alpha$  is a constant whose value was set to 0.6 for low vegetation.

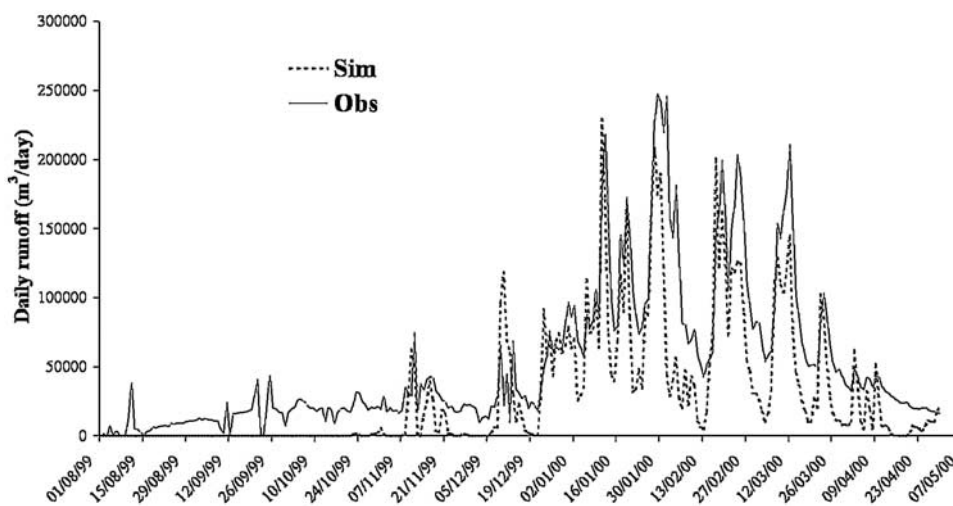


Figure 7. Initial runoff simulation without calibration at the outlet of the Liviñosa basin.

to this phenomenon was analyzed and a correction factor determined (see below, section 3.5.4).

### 3.5. Calibration and Validation

#### 3.5.1. Calibration Method and Steps

[29] The parameters were progressively calibrated, where each parameter of the model was analyzed separately. This method made it possible to assess the significance of each parameter relative to the model dynamics and, at the same time, to test the model's sensitivity to parameter variation [Braun and Renner, 1992]. Moreover, it avoided linking parameters that are normally not connected in the model [Tuteja and Cunnane, 1999].

[30] Various simulations with the parameter values ranging between two extreme values were carried out step by step following the decreasing sensitivity of the model. Since rock faces covered a large area in the basin (see Table 2), this type of surface was calibrated first in each calibration step. The quality of the model simulations was assessed using the simulated-to-observed runoff ratio (hereafter called  $R$ ), the Nash Efficiency Criterion (hereafter called  $E$ ) [Nash and Sutcliffe, 1970], the square root of the mean square error (hereafter called RMSE and stated in millimeters), and the correlation coefficient (hereafter called  $R^2$ ). The number of data points ( $n$ ) used for statistical calculations is recalled as well.

#### 3.5.2. Default Simulation and Process Description

[31] First, a default simulation was performed with the parameters set to their default value, presented in Tables 3 and 4. The flow routing scheme presented in Figure 5 was not considered at this stage; the runoff and drainage produced by each surface unit was simply added for each time step to calculate the resulting daily discharge at the basin outlet (both components were considered to integrate the hydrographic network and flow to the outlet of the basin in less than 1 day).

[32] Figure 7 shows the result of the default simulation. It can be observed that:

[33] • The seasonal dynamic observed is simulated reasonably well;

[34] • The simulated base flow runoff is too low.

[35] For this simulation,  $R = 0.57$ ,  $E = 0.58$ ,  $R^2 = 0.75$ , and  $RMSE = 2.69$  mm ( $n = 274$ ). Figure 8 shows the corresponding simulated surface ( $w_s$ ), root zone ( $w_2$ ), and deep soil water contents ( $w_3$ ), as well as the surface layer's

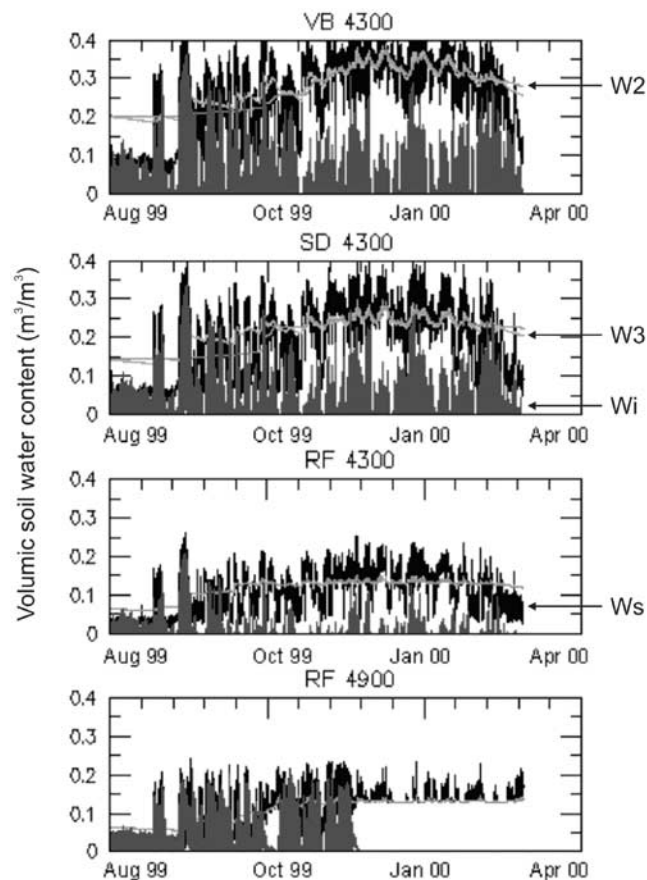
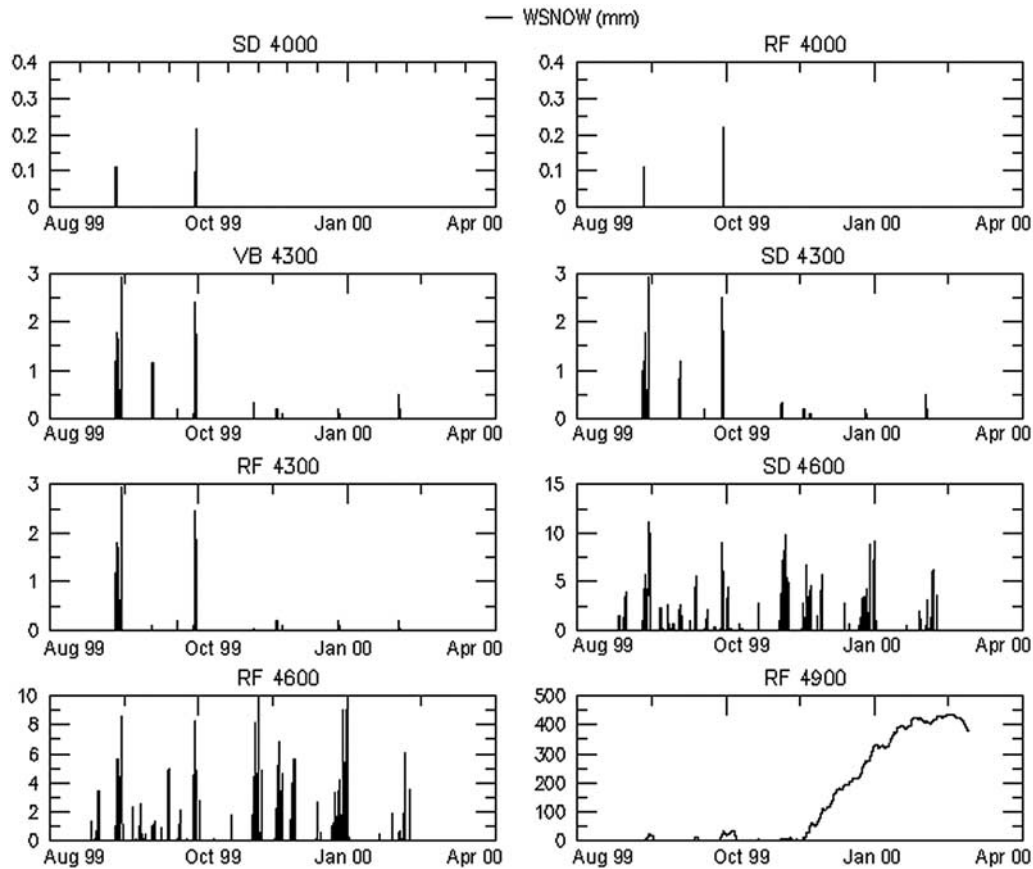


Figure 8. Liviñosa basin, volumic soil water content ( $m^3/m^3$ ) at the half-hour time step for four of the eight surface units (VB = valley bottom; SD = slope deposits; RF = rock faces).  $w_s$  is the surface layer water content,  $w_2$  the root zone water content,  $w_3$  the deep layer water content, and  $w_i$  the surface soil freezing water equivalent.



**Figure 9.** Snow water equivalent (mm) at the half-hour time step for the eight surface units describing the entire Liviñosa basin (VB = valley bottom; SD = slope deposits; RF = rock faces).

liquid water equivalent soil ice ( $w_i$ ) evolution for each surface unit. The surface soil water content ( $w_s$ ) varies significantly under the influence of the high temporal resolution atmospheric forcing, while the variations in deeper layer water content  $w_2$  and  $w_3$  fluctuations are lower because of the correspondingly thicker soil layers. The mean changes in the soil's water content in the three layers over the entire period follows the mean seasonal evolution of the atmospheric forcing, led by the alternating dry and rainy seasons.

[36] The influence of the soil texture on the soil water content's evolution in the different surface units can be observed in Figure 8. It can be seen, for example, that the valley bottom units contain more water than the rock face units, because the valley bottom units contain more finely textured soils (defined as a larger clay content), thereby retaining more water. The same remark can be made for the soil-freezing simulation, which is more intense for the high clay content units. However, the simulated soil freezing also varies according to the altitude of the surface unit. While no particular difference can be observed in terms of total soil water content between, for example, the rock face units at 4300 and 4600 m, a significantly higher soil freezing is simulated for the higher of the two surface units, because of the temperature decrease. As the soil-freezing processes have little influence on the runoff simulation at the daily time step [Cherkauer and Lettenmaier, 1999], it will not be further detailed in this study. It should be noted, however,

that the soil freezing increase with altitude ceases for the rock face unit at 4900 m, a result of the snow cover, which insulates the surface from the relatively cold atmospheric forcing and keeps the soil surface temperature close to 0°C.

[37] As can be seen in Figure 9, the end of the soil-freezing simulation on the rock face unit at 4900 m corresponds to the beginning of permanent snow cover. Even if the simulated snow logically increases with altitude starting from 4300 m, a rapid melt is simulated for altitudes lower than 4900 m. Indeed, this altitude roughly corresponds to the lower snow cover limit observed on the field. For the lower altitudes, the model simulates the significant impact of the atmospheric forcing, which prompts a rapid snowmelt (in particular, because of the atmospheric radiative forcing intensity and the relatively warm air temperatures). Finally, it is worth noting that, given the small fraction of the basin corresponding to the rock face unit at 4900 m (15% of the Liviñosa basin area), snow cover melting will moderately influence the hydrological behavior of the entire basin, as will be shown at the end of the next section.

### 3.5.3. Parameter Calibration

[38] Each parameter was calibrated step by step following the decreasing sensitivity of the model. The model's sensitivity, explored using the  $R$  and  $E$  criteria, was stronger for the variation in the subgrid drainage, followed by the soil depth and the subgrid runoff coefficient (see Figure 10).

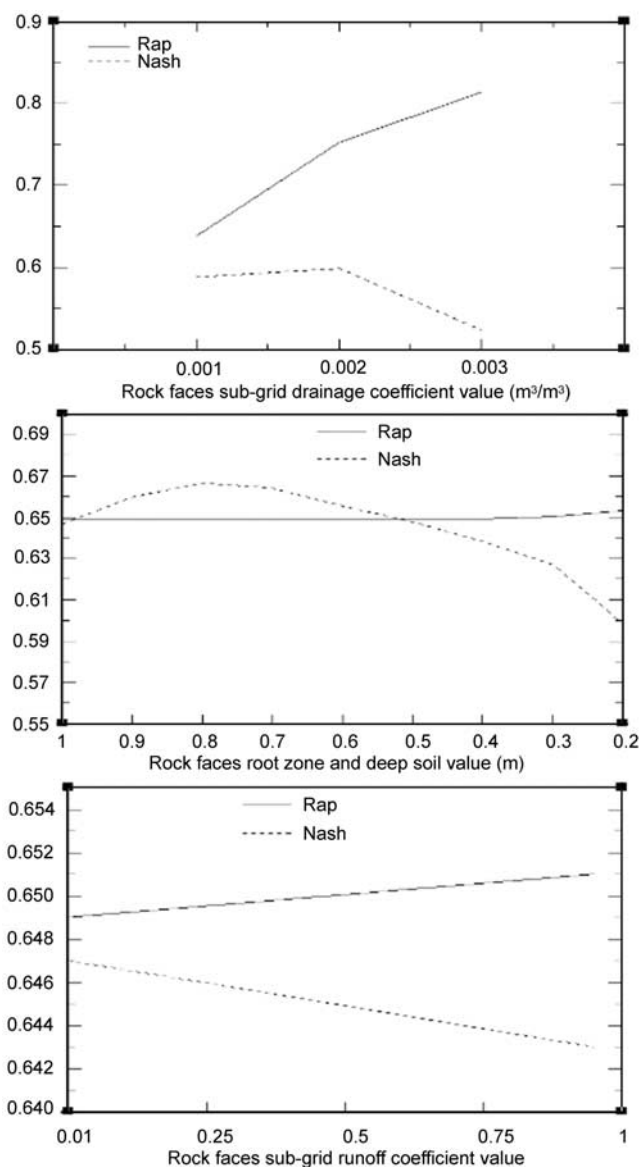


**Figure 10.** Calibration of the model's parameters for the rock face units qualified by the Rap and Nash values. The range of variation of these criteria illustrates the decreasing sensitivity of the model from the subgrid drainage to the subgrid runoff coefficient variation.

[39] Table 5 shows the main model's parameter and cumulated flux values obtained after calibration of the model's parameters. Note that the total precipitation decreased with altitude while the snowfall increased because of the decrease in temperature with altitude.

[40] The table also shows that the total evaporation varies more depending on the type of surface unit than as a function of altitude. The total evaporation simulated for the slope deposit units decreased with altitude, whereas it increased for the rock face units. This contrasting response was caused by two factors: (1) for the slope deposits, the soil water content decreased with altitude as a consequence of the decrease in precipitation and prompted a decrease in evaporation; (2) for the rock face units, the vegetation cover was considered to be negligible and only two layers were used to describe the soil,

which was relatively shallow compared to the slope deposit depth. Consequently, freezing in the rock face unit slowed drainage, thereby keeping more water in the deep layer and increasing the evaporation with altitude.

[41] Table 5 also shows that the permanent snow cover, simulated for the 4900-m rock face unit, blocked the soil evaporation flux. Note that the most significant component of the total evaporation over most of the units corresponds to the bare soil evaporation (especially for rock-face units which have no vegetation cover), except for the valley bottom units where similar values of transpiration were simulated.

[42] As stated in section 3.2, the distinction between snow and rain was determined using a critical temperature which was fixed according to the observations by *Leblanc* [2001]. In order to examine the sensitivity of the hydrological model of the basin to this critical temperature value, various simulations using critical temperature values ranging between  $-2^{\circ}$  and  $+2^{\circ}\text{C}$  were carried out. The resulting values of  $R$  and  $E$  are reported in Figure 11. As expected, because of the small fraction of the basin covered by snow (Figure 9), small differences were observed for values of the critical temperature lower than  $0.5^{\circ}\text{C}$ . For the unrealistic values over  $1^{\circ}\text{C}$ , a sharp decrease in the simulation quality occurred. This is consistent with the study by *L'Hôte et al.* [2004], who installed a complete weather station (including two rain gauge recorders, the first one based on weight measurement with added antifreeze and oil, and the other one with tipping buckets) at an altitude of 4800 m and 2 km to the south of the Plataforma station. This device provided a critical temperature of  $0.3^{\circ}\text{C}$  above which 100% of the precipitation falls as rain.

### 3.5.4. Regional Factors

[43] After the actual model calibration, the new statistical criterion values were  $R = 0.69$ ,  $E = 0.7$ ,  $R^2 = 0.81$ , and  $\text{RMSE} = 2.27$  mm ( $n = 274$ ). While the calibration improved the simulation results, the  $R$  value still reflected a large underestimation of the runoff. As the simulation was found to be coherent with the observed flow paths over each surface unit, we decided to analyze the regional factors that could influence the results, aiming to improve the final results (i.e., the criteria values) of the modeling approach.

[44] The first of these factors was the influence of the wind speed on the precipitation measurement. As stated above in section 3.4, the wind was known to cause a substantial underestimation in the measurement of the precipitation that actually falls into the basin. To test the sensitivity of the model to this factor and calculate the optimal correction to the measured rainfall, a new set of simulations was performed by increasing the total precipitation rate by factors ranging from 5 to 30%. As no reference device or data was available in this context to justify the choice of the correction factor before the calibration test, we decided to use a correction factor of 25%, for which the best simulated total discharge at the outlet of the basin was obtained ( $R = 0.98$ ,  $E = 0.76$ ,  $R^2 = 0.78$ , and  $\text{RMSE} = 2.05$  mm ( $n = 274$ )).

[45] The second regional factor taken into account was the routing of the water into the basin. In the aforementioned simulations, the water routing was simulated by adding the drainage and the runoff produced by each surface unit at the daily timescale, considering that the water transfer time into the basin is less than 1 day. In a high-mountain context, this hypothesis is generally true because

**Table 5.** Simulation Balance and Main Model Parameter Values for Each Surface Unit of the Liviñosa Basin After Calibration (V.B. - Valley Bottom; S.D. - Slope Deposits; R.F. - Rock Faces)

Surface Unit	S.D. 4000	R.F. 4000	V. B. 4300	S.D. 4300	R.F. 4300	S.D. 4600	R.F. 4600	R.F. 4900
Root Zone Depth	0.5	0.8	0.5	0.5	0.8	0.5	0.8	0.8
Deep Zone Depth	1	0.8	1	1	0.8	1	0.8	0.8
Subgrid Drainage Coeff.	0.001	0.002	0	0.001	0.002	0.001	0.002	0.002
Subgrid Runoff Coeff.	0.01	0.01	0.01	0.01	0.01	0.01	0.01	0.01
<i>Cumulated values over each surface unit after calibration</i>								
Total Precipitation, mm	1252	1252	1187	1187	1187	1122	1122	1057
Snowfall, mm	0	0	13	13	13	198	198	632
Rainfall, mm	1252	1252	1174	1174	1174	924	924	425
Total Precipitation on Snow, mm	0	0	14	14	15	218	221	947
Rainfall on Snow, mm	0	0	1	1	1	21	24	315
Snowfall on Snow, mm	0	0	13	13	13	198	198	632
Drainage, mm	720	965	612	675	895	629	814	481
Runoff, mm	4	2	7	4	2	4	2	0
Total Evaporation, mm	461	298	505	442	303	424	319	146
Soil Evaporation, mm	376	297	276	364	297	347	306	139
Vegetation Evaporation, mm	82	0	222	68	0	51	0	0

of the steep slopes of the landscape that cause rapid water transfer. However, the slope deposits observed in the basin were found to be able to delay the water transfer by more than 1 day, particularly before and after the rainy season [Caballero *et al.*, 2002]. In the field, at the beginning of the rainy season, it was observed that all the water flowing from the rock faces could infiltrate through the moraine material, the slope deposits, or within the valley bottom peat and reappear downstream in water sources. To take this phenomenon into account, a water transfer scheme, called the “cascade routing scheme,” was added to the model. This scheme simply introduces the water produced by the rock face units into the corresponding lower elevation slope deposit units and then the water produced by the latter into the valley bottom unit.

[46] As a result, the flow paths between the different units were organized following two simple rules:

[47] ● The water produced in a given surface unit must be introduced in a surface unit located at a lower elevation band (i.e., no lateral transfer allowed).

[48] ● Whenever possible, the water from the rock faces must be introduced into the slope deposits and then into the valley bottom.

[49] The water flowing from an upper unit was introduced at an equal rate in both the root zone and the deep layers of the lower elevation unit. When the soil water content reached the saturation point, the water in excess was considered to be surface runoff. The resulting flow path organization can be observed on the right side of Figure 5. With this routing scheme, the outlet of the subbasin, located in the valley bottom surface unit at 4000 m, received the water which transited all of the upper surface units. This more realistic routing scheme improved the statistical criteria values as  $R = 0.99$ ,  $E = 0.84$ ,  $R^2 = 0.86$ , and  $RMSE = 1.65$  mm ( $n = 274$ ).

[50] Figure 12 shows the result of the simulation with adjusted precipitation and the cascade routing scheme.

### 3.5.5. Validation Results

[51] The validation simulation was conducted over the year following the calibration period (Figure 13). An important gap appeared in the observed discharge record

in the middle of the 2001 rainy season. Figure 13 shows that the general trend of the observed discharge was rather well simulated, in particular, for the beginning and the end of the rainy season (gray arrows). This figure also presents the Liviñosa reservoir’s influence on the observed discharge, which increased during the reservoir-emptying period (between black arrows) because of the water release. The model simulates the natural behavior of the basin in that it does not integrate the reservoir influence. In particular, it simulates the flood corresponding to the precipitation event observed at the end of the dry season (right black arrow). This flood was not recorded by the water level gauge at the outlet of the basin because it occurred during the beginning of the filling of the reservoir. The statistical criteria values obtained for this simulation over periods where observed discharge

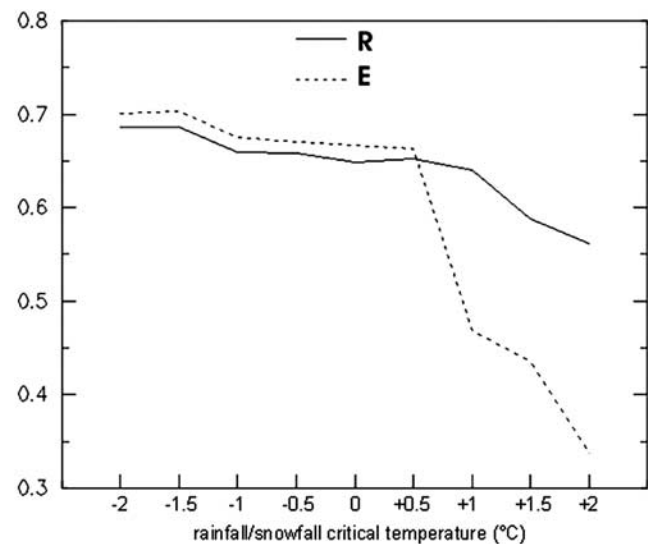


**Figure 11.** Sensitivity test of the calibrated model to the rainfall/snowfall critical temperature variation; the closer the runoff ratio ( $R$ ) and the Nash criteria ( $E$ ) are to 1, the better the model simulates the discharge at the outlet of the basin. The critical temperature value varies between  $-2^{\circ}\text{C}$  and  $+2^{\circ}\text{C}$ .

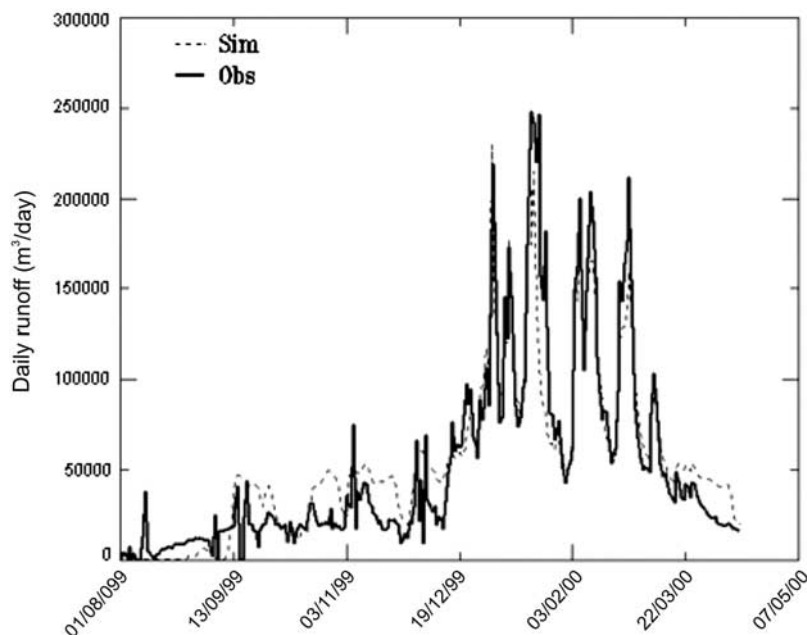


**Figure 12.** Simulation of the discharge at the basin’s outlet with the calibrated model, 25% precipitation correction, and the new routing scheme.

was both available and not influenced by the reservoir (that is, from 1 April 2000 to 23 July 2000, 10 December 2000 to 28 December 2000, and 10 March 2001 to 31 March 2001) were  $R = 1.09$ ,  $E = 0.86$ ,  $R^2 = 0.88$ , and  $RMSE = 0.96$  mm ( $n = 155$ ). These results validated the modeling method over the Liviñosa basin. Consequently, it was successfully applied, with the same parameterization, to the entire Zongo River upper basin with the objective of building a decision support tool [Caballero *et al.*, 2004].

**4. Conclusions**

[52] This paper presents an application of the soil-atmosphere-vegetation transfer scheme, ISBA, for hydro-

meteorological modeling purposes. It focuses on two original features: (1) the extreme conditions experienced in a small tropical mountain river basin located above 3500 m asl in the Cordillera Real of the Andes in Bolivia; and (2) the use of a nongridded representation method, instead of the regular and homogeneous square grid usually used for this type of model. This second feature is a consequence of the first one.

[53] The extreme conditions experienced in the basin studied generated several problems: (1) extreme atmospheric forcing due to the tropical high-mountain context (rainfall/snowfall, temperature, humidity, wind speed, and solar and atmospheric radiation); (2) the influence of altitude, steep slopes, and hillside orientation; (3) the inaccuracy of the

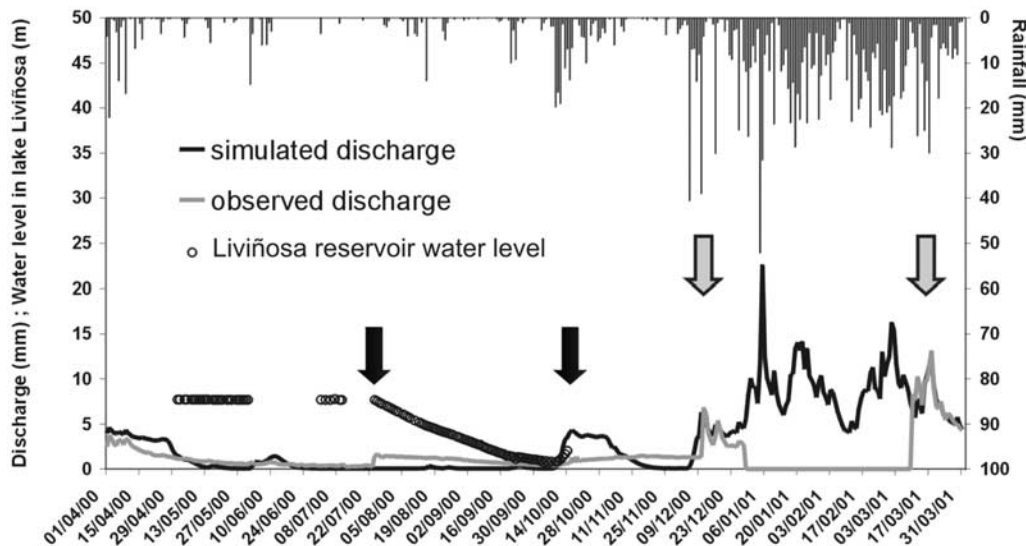


**Figure 13.** Comparison of the simulated to the observed discharge at the outlet of the basin and to the Liviñosa reservoir water level evolution.

observed data, because of difficult access to the field, which needed spatial extrapolations with data recorded at a certain distance from the basin; and (4) the presence of hydraulic devices modifying the natural flow regime.

[54] Even if the basin's area was small (12.5 km<sup>2</sup>), it was necessary to take the above mentioned characteristics into account, as well as the different types of soil and the water routing through the basin, which resulted in eight surface units, crossing elevation bands with three types of morphological features.

[55] The seasonal evolution of the soil's water content was simulated for each surface unit. The extreme atmospheric forcing led to a substantial variation in the soil's water content in the surface soil layer, while the latter had a protective effect for the deeper layers. Simulated soil water content and freezing was greater for finely textured soils, the latter increasing with altitude, while it was stopped when snow covered the surface. A critical altitude of 4900 m was found to be the limit over which a permanent snow cover is simulated. As a consequence, the river basin surface permanently covered by snow was limited and the snowmelt had a moderate influence on the river flow regime.

[56] A progressive calibration of the subgrid drainage, soil depth, and subgrid runoff was undertaken starting from the type of soil surface covering the higher area (rock faces) in the basin. Regional factors such as the influence of wind speed and a specific flow routing scheme (the default was based on the addition of the runoff and drainage produced by each surface unit at the daily timescale) were necessary to optimize the calibration.

[57] Simulating the river discharge over 1 year following the calibration period allowed us to validate the model and extend it to a larger basin scale, following a decision support system perspective [Caballero et al., 2004]. The wide use of the mountain flows for agriculture, animal breeding, energy production, and domestic water supply in the countries of the Pacific dry side of the Andes give particular importance to being able to properly simulate the hydrological processes in this context. An ongoing project initiated in 2005 will extend this approach to a neighboring watershed including a glacier, where another surface scheme (CAB) [Ducharne et al., 2000; Koster et al., 2000] will be tested to compare their performance.

[58] **Acknowledgments.** In Bolivia, the following institutions and scientific institutes supported fieldwork: the Bolivian Power Company, the Hydraulics and Hydrology Institute, Universidad Mayor San Andrés of La Paz and the local representation of Institut de Recherche pour le Développement (IRD, France). In France, this study was able to use the facilities offered by IRD, Météo France, Bureau de Recherche Géologique et Minière, and Centre National de la Recherche Scientifique. We also thank Jean-Philippe Chazarin, Rolando Fuertes, Robert Gallaire, Yann L'Hôte, Ramiro Pillco, and Bernard Pouyau, who helped a lot for the field works, and Jean-Marc Leblanc and Igor Rheinhardt, whose studies were preliminary approaches of the present one. Finally, we are grateful to the three anonymous reviewers who made a very detailed and consistent analysis; they helped us better organize our paper and focus it more clearly on its main topic.

## References

- Aceituno, P. (1988), On the functioning of the southern oscillation in the South American sector. Part I: Surface climate, *Mon. Weather Rev.*, *116*, 505–524.
- Barnett, T. P., J. C. Adam, and D. P. Lettenmaier (2005), Potential impacts of a warming climate on water availability in snow-dominated regions, *Nature*, *438*(17 November 2005), 303–309.
- Barry, R. G. (1992), *Mountain Weather and Climate*, Routledge Physical Environment Series, London.
- Boone, A. (2000), Modélisation des processus hydrologiques dans le schéma de surface ISBA: Inclusion d'un réservoir hydrologique, du gel et modélisation de la neige. Thèse Université Paul Sabatier (Toulouse III).
- Boone, A., and P. Etchevers (2001), An inter-comparison of three snow schemes of varying complexity coupled to the same land-surface model: Local scale evaluation at an Alpine site, *J. Hydrometeorol.*, *2*, 374–394.
- Boone, A., J. C. Calvet, and J. Noilhan (1999), Inclusion of a third soil layer in a land surface scheme using the force-restore method, *J. Appl. Meteorol.*, *38*, 1611–1630.
- Boone, A., V. Masson, T. Meyers, and J. Noilhan (2000), The influence of the inclusion of soil freezing on simulations by a Soil-Vegetation-Atmosphere transfer scheme, *J. Appl. Meteorol.*, *39*, 1544–1569.
- Boone, A., et al. (2004), The Rhone aggregation land surface scheme intercomparison project: an overview, *J. Clim.*, *17*(1), 187–208.
- Bowling, L. C., et al. (2003), Simulation of high-latitude hydrological processes in the Torne-Kalix Basin; PILPS Phase 2(e); 1, Experiment description and summary intercomparisons; Project for Intercomparison of Landsurface Parameterization Schemes, Phase 2(e), *Global Planet. Change*, *38*(1-2), 1–30.
- Braun, L. N., and C. B. Renner (1992), Application of a conceptual runoff model in different physiographic regions of Switzerland, *Hydrol. Sci. J.*, *37*(3), 217–231.
- Brutsaert, W. (1982), *Evaporation Into the Atmosphere*, Springer, New York.
- Caballero, Y. (2001), Modélisation des écoulements d'origine pluvio-nivo-glaciaire en contexte de haute montagne tropicale. Application à la haute vallée du Rio Zongo (Bolivie), Thèse, Institut des Sciences de la Terre de l'Eau et de l'Espace de Montpellier (ISTEEM). (<http://www.mpl.ird.fr/hydrologie/pch/documents/mayu.html>)
- Caballero, Y., V. Jomelli, P. Chevallier, and P. Ribstein (2002), Hydrological characteristics of slope deposits in high tropical mountains (Cordillera Real, Bolivia), *Catena*, *47*(2), 101–116.
- Caballero, Y., P. Chevallier, R. Gallaire, and R. Pillco (2004), Flow modelling in a high mountain valley equipped with hydropower plants: Rio Zongo Valley, Cordillera Real, Bolivia, *Hydrol. Process.*, *18*, 939–957.
- Caballero, Y., S. Voirin-Morel, F. Habets, J. Noilhan, P. LeMoigne, A. Lehenaff, and A. Boone (2007), Hydrological sensitivity of the Adour-Garonne river basin to climate change, *Water Resour. Res.*, doi:10.1029/2005WR004192, in press.
- Calvet, J. C., J. Noilhan, P. Bessemoulin, M. Cabelguenne, A. Olioso, and J. P. Wigneron (1998), An interactive vegetation SVAT model tested against data from six contrasting sites, *Agric. For. Meteorol.*, *92*, 73–95.
- Chang, M., and L. A. Flanery (2001), Spherical gauges for improving the accuracy of rainfall measurements, *Hydrol. Process.*, *15*, 643–654.
- Cherkauer, K. A., and D. P. Lettenmaier (1999), Hydrologic effects of frozen soils in the upper Mississippi River basin, *J. Geophys. Res.*, *104*(D16), 297–317.
- Chevallier, P., and J. M. Lapetite (1986), Note sur les écart de mesure observés entre les pluviomètres standards et les pluviomètres au sol en Afrique de l'Ouest, *Hydrol. Cont.*, *1*(2), 111–119.
- Deardorff, J. W. (1977), A parameterization of ground-surface moisture content for use in atmospheric prediction models, *J. Appl. Meteorol.*, *16*, 1182–1185.
- Deardorff, J. W. (1978), Efficient prediction of the ground surface temperature and moisture with inclusion of a layer of vegetation, *J. Geophys. Res.*, *83*(C4), 1889–1903.
- Dirmeyer, P., A. J. Dolman, and N. Sato (1999), The global soil wetness project: A pilot project for global land surface modeling and validation, *Bull. Am. Meteorol. Soc.*, *80*, 851–878.
- Douville, H., J.-F. Royer, and J. F. Mahfouf (1995), A new snow parameterization for the Meteo-France climate model. Part I: Validation in stand-alone experiments, *Clim. Dyn.*, *12*, 21–35.
- Ducharne, A., R. D. Koster, M. J. Suarez, M. Stieglitz, and P. Kumar (2000), A catchment-based approach to modelling land surface processes in a general circulation model. 2: Parameter estimation and model demonstration, *J. Geophys. Res.*, [Atmos.], *105*(D20), 24,823–24,838.
- Dümenil, L., and E. Todini (1992), A rainfall-runoff scheme for use in the Hamburg climate model, in *Advances in Theoretical Hydrology*, a tribute to James Dooge, vol., edited by McGraw-Hill, pp. 129–157, New York.
- Dunne, T., and R. Black (1970), An experimental investigation of runoff production in permeable soils, *Water Resour. Res.*, *6*(2), 478–490.
- Etchevers, P. (2000), Modélisation du cycle continental de l'eau à l'échelle régionale. Impact de la modélisation de la neige sur l'hydrologie du Rhône, thèse, Université de Toulouse III.

- Etchevers, P., C. Golaz, and F. Habets (2001), Simulation of the water budget and the river flows of the Rhône basin from 1981 to 1994, *J. Hydrol.*, *244*, 60–85.
- Favier, V., P. Wagnon, and P. Ribstein (2004), Glaciers of the outer and inner tropics: A different behaviour but a common response to climate forcing, *Geophys. Res. Lett.*, *31*(16), L16403, doi:10.1029/2004GL020654.
- Flamiglietti, J. S., and E. F. Wood (1994), Multiscale modeling of spatially variable water and energy balance processes, *Water Resour. Res.*, *30*, 3061–3078.
- Francou, B., E. Ramirez, B. Caceres, and J. Mendoza (2000), Glacier evolution in the tropical Andes during the last decades on the 20th Century: Chacaltaya, Bolivia and Antizana, Ecuador, *Ambio*, *29*(7), 416–422.
- Giard, D., and E. Bazile (2000), Implementation of a new assimilation scheme for soil and surface variables in a global NWP model, *Mon. Weather Rev.*, *128*, 997–1015.
- Habets, F., P. Etchevers, C. Golaz, E. Leblois, E. Ledoux, E. Martin, J. Noilhan, and C. Otle (1999a), Simulation of the water budget and the river flows of the Rhone basin, *J. Geophys. Res.*, *104*, 31,145–31,172.
- Habets, F., J. Noilhan, C. Golaz, J. P. Goutorbe, P. Lacarrere, E. Leblois, E. Ledoux, E. Martin, C. Otle, and D. Vidal-Madjar (1999b), The Isba surface scheme in a macroscale hydrological model applied to the Hapex-Mobilhy area. Part I: Model and database, *J. Hydrol.*, *217*, 75–96.
- Habets, F., J. Noilhan, C. Golaz, J. P. Goutorbe, P. Lacarrere, E. Leblois, E. Ledoux, E. Martin, C. Otle, and D. Vidal-Madjar (1999c), The Isba surface scheme in a macroscale hydrological model applied to the Hapex-Mobilhy area. Part II: Simulation of streamflows and annual water budget, *J. Hydrol.*, *217*, 97–118.
- Henderson-Sellers, A., Z. L. Yang, and R. E. Dickinson (1993), The Project for Intercomparison of Land-Surface Parameterization Schemes PILPS, *Bull. Am. Meteorol. Soc.*, *74*, 1335–1349.
- Henderson-Sellers, A., A. J. Pitman, P. Love, P. Irannejad, and T. Chen (1995), The project of intercomparison of land-surface parameterization schemes (PILPS): Phases 2 and 3, *Bull. Am. Meteorol. Soc.*, *94*, 489–503.
- Horton, R. E. (1945), Erosional development of streams and their drainage basins: Hydrophysical approach to quantitative morphology, *Bull. Geol. Soc. Am.*, *56*, 275–370.
- Koster, R. D., M. J. Suarez, A. Ducharme, M. Stieglitz, and P. Kumar (2000), A catchment-based approach to modelling land surface processes in a general circulation model. 1: Model structure, *J. Geophys. Res.*, [Atmos.], *105*(D20), 24,809–24,822.
- Leblanc, J. M. (2001), Dynamique de la couverture neigeuse dans les Alpes Tropicales. Mémoire de DEA, Université Montpellier II.
- L'Hôte, Y., P. Chevallier, P. Etchevers, Y. Lejeune, and P. Wagnon (2004), Rainfall or snowfall? Device for measuring the precipitation phase in the Bolivian Andes and analysis of the records, *Hydrol. Sci. J.*, *49*(2), 237–281.
- Mahfouf, J.-F., and J. Noilhan (1996), Inclusion of gravitational drainage in a land surface scheme based on the force-restore method, *J. Appl. Meteorol.*, *35*, 987–992.
- Nash, J. E., and J. V. Sutcliffe (1970), River flow forecasting through conceptual models, *J. Hydrol.*, *10*(3), 282–290.
- Noilhan, J., and P. Lacarrère (1995), GCM grid-scale evaporation from mesoscale modelling, *J. Clim.*, *8*, 206–223.
- Noilhan, J., and J.-F. Mahfouf (1996), The ISBA land surface parameterization scheme, *Global Planet. Change*, *13*, 145–159.
- Noilhan, J., and S. Planton (1989), A simple parameterization of Land Surface Processes for meteorological Models, *Mon. Weather Rev.*, *117*, 536–549.
- Reinhardt, I. (1997), Analyse des composantes naturelles et artificielles de la ressource en eau de la vallée du Zongo en Bolivie, IRD, Montpellier, Mémoire Post-grade. Ecole Polytechnique Fédérale de Lausanne, Suisse.
- Ribstein, P., E. Tiriau, B. Francou, and R. Saravia (1995), Tropical climate and glacier hydrology: A case study in Bolivia, *J. Hydrol.*, *165*, 221–234.
- Roche, M. A. (1982), Les conditions d'une étude hydrologique en Amazonie bolivienne. Rapport ORSTOM, La Paz, Bolivie.
- Royer, J. F., et al. (2002), Simulation des changements climatiques au cours du 21<sup>me</sup> siècle incluant l'ozone stratosphérique, *Compte Rendus de Géoscience*, *334*(3), 147–154.
- Schlosser, C. A., A. G. Slater, A. Robock, A. J. Pitman, K. Y. Vinnikov, A. Henderson-Sellers, N. A. Speranskaya, and K. Mitchell (2000), Simulations of a boreal grassland hydrology at Valdai, Russia: PILPS Phase 2 (d), *Mon. Weather Rev.*, *128*, 301–321.
- Sicart, J. E., P. Wagnon, and P. Ribstein (2005), Atmospheric controls of the heat balance of Zongo Glacier (16 degrees S. Bolivia), *J. Geophys. Res.*, [Atmos.], *110*(D12).
- Staley, D. O., and G. M. Jurica (1972), Effective atmospheric emissivity under clear skies, *J. Appl. Meteorol.*, *11*(349), 3561972.
- Tuteja, N. K., and C. Cunnane (1999), A quasi physical snowmelt runoff modelling system for small catchments, *Hydrol. Process.*, *13*, 1961–1975.
- Voirin-Morel, S. (2003), Modélisation distribuée des flux d'eau et d'énergie et des débits à l'échelle régionale du bassin Adour Garonne, PhD, Université Paul Sabatier, Météo-France, Toulouse.
- Vuille, M., R. S. Bradley, and F. Keimig (2000), Interannual climate variability in the Central Andes and its relation to the tropical Pacific and Atlantic forcing, *J. Geophys. Res.*, [Atmos.], *105*(D10), 12,447–12,460.
- Wagnon, P., P. Ribstein, G. Kaser, and P. Berton (1999), Energy balance and runoff seasonality of a Bolivian glacier, *Global Planet. Change*, *22*(1-4), 48–59.
- Wood, E. F., D. P. Lettenmaier, and V. Zartarian (1992), A land-surface hydrology parameterization with sub-grid variability for general circulation models, *J. Geophys. Res.*, *97*(D3), 2717–2728.
- Wood, E. F., et al. (1998), The project for intercomparison of land-surface parameterization scheme (PILPS) Phase 2 (c) Red-Arkansas river experiment: I. Experiment description and Summary intercomparisons, *Global Planet. Change*, *19*, 115–136.
- Yang, D., et al. (1999), Quantification of precipitation measurement discontinuity induced by wind shields on national gauges, *Water Resour. Res.*, *35*(2), 491–508.
- Yang, D., D. L. Kane, L. D. Hinzman, B. E. Goodison, J. R. Metcalfe, P. Y. T. Louie, G. H. Leavesley, D. G. Emerson, and C. L. Hanson (2000), An evaluation of the Wyoming gauge system for snowfall measurement, *Water Resour. Res.*, *36*(9), 2665–2677.

A. Boone and J. Noilhan, Centre National de Recherches Météorologiques Météo-France, Toulouse, France.

Y. Caballero, Bureau de Recherche Géologique et Minière Corse, Immeuble Agostini, ZI Furiani, 20600 Bastia, France. (y.caballero@brgm.fr)

P. Chevallier, Institut de Recherche pour le Développement Great Ice, Montpellier, France.

F. Habets, UMR Sysiphe, CNRS, Université Pierre et Marie Curie, Paris, France.